



# Adaptive Slicing and Process Optimization for Direct Metal Deposition to Fabricate Exhaust Manifolds

Daniel Eisenbarth<sup>1</sup>(✉) , Alessandro Menichelli<sup>2</sup>, Fabian Soffel<sup>1</sup> ,  
and Konrad Wegener<sup>2</sup>

<sup>1</sup> Inspire AG, ETH Zurich, Zurich, Switzerland  
[eisenbarth@inspire.ethz.ch](mailto:eisenbarth@inspire.ethz.ch)

<sup>2</sup> Institute of Machine Tools and Manufacturing, ETH Zurich, Zurich, Switzerland  
<https://www.inspire.ethz.ch/>

**Abstract.** Direct metal deposition is an additive technology that has the potential to fabricate large parts in multiple buildup directions. Especially curved, thin-walled geometries such as exhaust manifolds are a promising use case: In theory, direct metal deposition allows nearly arbitrary shapes. Internal surfaces that are not accessible with the final part could be inspected and machined in a stepwise buildup process. However, the successful production of such parts requires suitable algorithms for five-axis tool path planning as well as for the optimization of the parameters for the specific process. Herein, an adaptive slicing algorithm is presented that aligns the direction of each layer for minimized overhangs and creates the tool path under consideration of the process capabilities and limits. By a variation of the scan speed, the deposited powder per length and therefore the layer height can be modified continuously. A model-based feedforward control of the laser power accounts for the varying thermal conduction in thin walls. These approaches are integrated in a fully automated CAM software that generates a suitable tool path with locally adapted parameters. The fabrication of an exemplary exhaust manifold shows that the software reduces the manual preparation effort and enables a flexible additive manufacturing process.

**Keywords:** Direct metal deposition · Adaptive slicing · Tool path planning · Process optimization · CAM programming

## 1 Introduction

Additive manufacturing (AM) of metals is currently dominated by powder-bed technologies. Although they show various advantages, there are process-inherent drawbacks such as the predefined, vertical buildup direction and the necessity of support structures to fabricate overhanging walls above a critical angle. While powder-bed AM is characterized by the two steps of powder placement and fusion, there are various deposition welding technologies that feed the material directly into the melt pool. With these AM processes, both the energy and

material are delivered by a single processing head, which is mostly attached to a robot or CNC machine. Thus, only the axis range limits the design space, and multi-axis systems allow an arbitrary orientation of the processing head relative to the workpiece. This flexibility promises the additive production of large parts without the need for support structures as demonstrated by Greer et al. [1]. As of today, deposition welding is applied in the industry mainly for coatings and the repair of geometrically simple elements as shown by Petrat et al. [2]. The fabrication of complex, multi-layer structures in arbitrary buildup directions is still in an early research phase, as it poses various challenges that need to be solved. These challenges can be divided into digital and physical issues: First, a suitable and collision-safe tool path needs to be calculated from a CAD model, ideally in an automated approach. Second, the applied deposition welding process needs to be able to manufacture the part with the desired microstructure, surface roughness, and geometrical accuracy. A common depositing welding technology is direct metal deposition (DMD) as used in here, where metallic powder is blown by a gas stream into a melt pool created by a laser beam.

Figure 1 presents eight generic slicing approaches to create layers from a 3D model, depending on the ability of the tool path to change the buildup direction and on the ability of the process to vary the layer height locally. Three levels of complexity are distinguished here. The easiest approach of a constant layer direction and height is shown by illustration (a), with the layers marked in gray and black on a white substrate. By dividing the part into sub-volumes as shown in (b), the buildup direction can be optimized for each geometrical element in order to prevent overhangs or to improve the surface roughness as performed by Ding et al. [3] and Murtezaoglu et al. [4]. The tool path calculation becomes most complex when the direction changes within one layer. This approach is required for AM processes that start on a curved substrate as shown by Zhao et al. [5]. With a constant layer height as illustrated in (c), each layer is an offset of the initial substrate curvature.

If it is possible to change the deposition height during the process, the staircase effect that occurs at slopes and overhangs can be reduced by a variable height from layer to layer as proposed by Mao et al. [6] and shown in (d). Illustrations (e) and (f) depict combinations of the previously explained approaches. Multidirectional but plane slicing is illustrated in (g). By a continuous adaptation of the buildup direction, overhangs and the staircase effect can be prevented for parts that tilt gradually from the bottom to the top. This approach requires a local adaptation of the layer height, which can be achieved for instance by a variation of the track overlap or the deposition rate per length. An alternative is to generate a sloped surface by a staircase, consisting of multiple sub-layers. Chalvin et al. [7] and Wang et al. [8] implement the slicing approach (g) for polymer-based filament AM. Ruan et al. [9] perform adaptive slicing with metals, but create the required slope by milling of each layer. The difficulty of adaptive slicing in combination with DMD is the dynamic control of the layer height while ensuring similar process conditions without over- or underheating

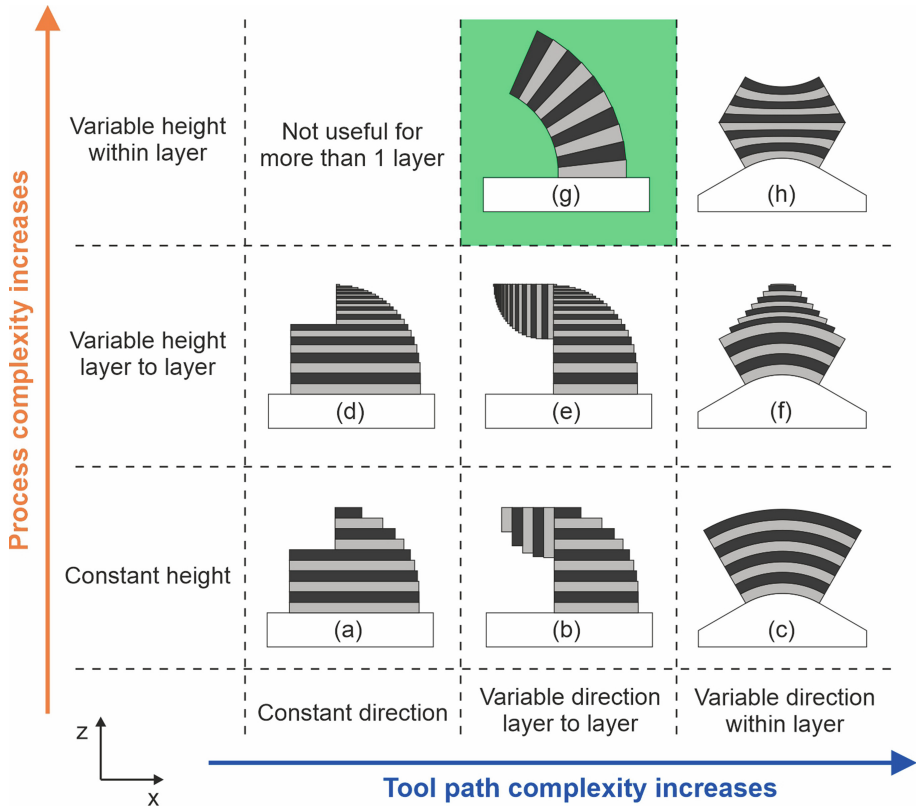


Fig. 1. Generic slicing approaches with a varying tool path and process complexity

of the part. Varying both the buildup direction and the layer height as shown in (h) is demonstrated with a simple tube by Wang et al. [10].

## 2 Materials and Methods

This publication deals with adaptive slicing according to approach (g) in combination with a five-axis tool path, demonstrated by the fabrication of a twisted, thin-walled exhaust manifold. Material scientific issues are not discussed. However, the part geometry influences the processing conditions as outlined by Eisenbarth et al. [11]. A nearly steady-state DMD process can only be achieved by an adaptation of the critical process parameters. Here, a model-based feed-forward control method is applied to optimize both the laser power and the scan speed according to the local process requirements. These approaches are integrated in a fully automated CAM software as developed in-house using MATLAB. Figure 2 shows a simplified flowchart of the adaptive slicing algorithm within the CAM software architecture, highlighted in gray. The subsequent mod-

ules calculate the tool path and the process parameters before the NC-code is created. The depicted algorithm is explained in the following sections.

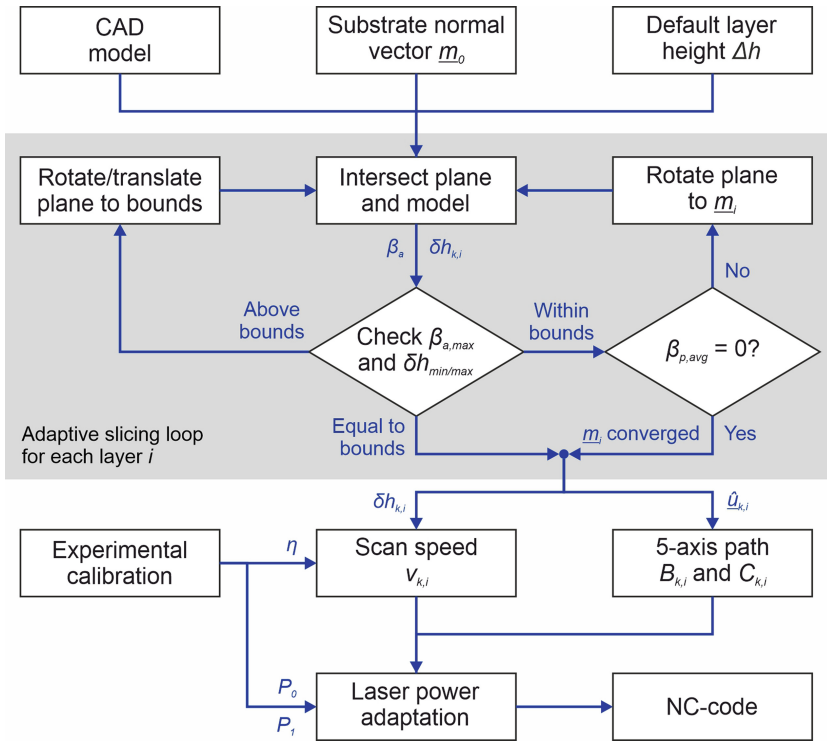


**Fig. 2.** Flowchart of the adaptive slicing loop and its integration in the CAM software

## 2.1 Concept of Adaptive Slicing

An inclined slicing plane with layer number  $i$  is defined by a position and a normal vector  $\underline{m}_i$ , which are calculated from the 3D model to be built. The STL file format is used as input, as it is widespread, independent from specific CAD modeling methods, and simple to decompose. Various approaches exist to determine the normal vector: The centerline of a part can be imported from a CAD software or calculated explicitly as done by Ruan et al. [12]. Problems occur as soon as the part splits into or merges from multiple sub-volumes. An alternative is to focus on the DMD process requirements, namely on minimizing the overhang angles independent of any centerline. It is possible to minimize the maximum overhang angle as done by Ding et al. [3], to use a certain cost function, or to minimize the average overhang angle per path length as performed herein.

In addition, the process limits in terms of the minimum and maximum achievable layer heights  $\delta h_{min}$  and  $\delta h_{max}$  need to be considered by the slicing algorithm. The maximum tilt angle  $\beta_{a,max}$  is an inverse tangent function of the maximum layer height difference divided by the maximum part width  $w_{prt}$  in the tilting direction:

$$\beta_{a,max} = \tan^{-1} \left( \frac{\delta h_{max} - \delta h_{min}}{w_{prt}} \right) \quad (1)$$

The most inward wall of the part can show a minimum surface radius  $r_{a,min}$ , approximated as

$$r_{a,min} = \frac{\delta h_{min}}{\beta_{a,max}} \quad (2)$$

Thus, the achievable surface radius is constrained by the DMD process capabilities and the part width in the tilting direction. The normal vector  $\underline{m}_i$  is determined in an iterative process: In the first iteration, the part is sliced parallel to the previous layer  $i - 1$  in a default distance  $\Delta h$  as shown in illustration (a) of Fig. 3. The gray volume depicts the cross-section of an arbitrary part in the  $xz$ -plane.

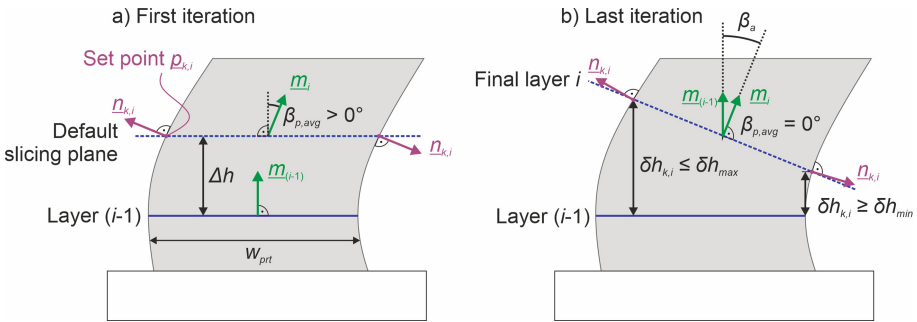


**Fig. 3.** Adaptive slicing in an iterative process: Calculation of the intended normal vector  $\underline{m}_i$  (a), translating and rotating until a convergence criterion is met (b)

The intersection of the plane with the triangles of the STL geometry results in one or more closed contour paths, defined by set points  $\underline{p}_{k,i}$  for each intersection  $k$  in layer  $i$ . The total number of points in one layer is denoted as  $N$ . The path from one set point to the next can be written as path segment vector  $\underline{u}_{k,i}$  with a related normal vector  $\underline{n}_{k,i}$  of the respective triangle that defines the wall orientation. The average wall direction is calculated as the sum of the cross products of  $\underline{u}_{k,i}$  and  $\underline{n}_{k,i}$ , corresponding to normal vector of the new slicing plane  $\underline{m}_i$ :

$$\underline{m}_i = \sum_{k=1}^N (\underline{u}_{k,i} \times \underline{n}_{k,i}) \quad (3)$$

Since  $\underline{n}$  is a unit vector and  $\underline{u}$  is the path segment length, the direction of  $\underline{m}_i$  is weighted inherently according to the respective path distances. The average wall inclination  $\beta_{p,avg}$  is the angle between the normal vectors of two iterations. As long as this angle is larger than 0, a mismatch exists between the slicing orientation and the average wall inclination. The intersection of the new slicing plane with the STL geometry creates a different contour path that can result in a varying normal vector  $\underline{m}_i$ . Thus, this algorithm is repeated until  $\beta_{p,avg}$  is 0 or complies to a certain convergence criterion as shown in illustration (b) of Fig. 3. From the previous to the next slicing plane as well as from one iteration to another, the angle  $\beta_a$  between two normal vectors  $\underline{m}_{i-1}$  and  $\underline{m}_i$  is calculated with the dot product:

$$\beta_{a,i} = \cos^{-1} \left( \frac{\underline{m}_i \cdot \underline{m}_{i-1}}{|\underline{m}_i| \cdot |\underline{m}_{i-1}|} \right) \quad (4)$$

At the same time, the algorithm needs to ensure that the local layer height  $\delta h_{k,i}$  at each set point  $\underline{p}_{k,i}$  lies within the layer height limits of the process. If these limits are exceeded, the plane is translated and rotated accordingly, considering the maximum tilt angle  $\beta_{a,max}$ . The local layer height can be calculated with the law of conservation of mass, assuming a constant total powder flow rate  $\dot{m}$ , a constant powder catchment efficiency  $\eta$  as the fraction of the powder reaching the melt pool, and a constant density  $\rho$  of the solid material. If a thin wall is made of stacked DMD tracks with an average wall width  $w_m$ , the local layer height is inversely proportional to the local scan speed  $v$  at a set point  $\underline{p}_{k,i}$ :

$$\delta h_{k,i} = \frac{\dot{m} \cdot \eta}{w_m \cdot \rho} \cdot v_{k,i}^{-1} \quad (5)$$

The volumetric energy density  $e_v$  describing the heat input for a certain volume of deposited material is calculated as:

$$e_v = \frac{P}{v_{k,i} \cdot w_m \cdot \delta h_{k,i}} = \frac{P \cdot \rho}{\dot{m} \cdot \eta} \quad (6)$$

It can be seen that  $e_v$  does not depend on the local scan speed. Since a local variation of the layer height does not influence the amount of deposited material per time, it is reasonable to apply a constant laser power  $P$  to maintain a constant volumetric energy density. However, the specific energy  $e_a$  as a measure for the heat input on a certain workpiece area is a function of  $v$ :

$$e_{a,k,i} = \frac{P}{w_m} \cdot v_{k,i}^{-1} \quad (7)$$

Thus, the process window for a varying layer height is constrained by the minimum and maximum scan speeds that allow a proper bonding to the last layer. Furthermore, the maximum tilt angle  $\beta_{a,max}$  of a plane is limited by the dynamics of the DMD process: Since the melt pool is liquid, the amount of deposited powder per length is averaged within the area of the melt pool.

Thus, a rapidly changing scan speed will not lead to the same dynamic response of the local layer height.

If the radius  $r_a$  of the CAD model is smaller than the minimum achievable radius  $r_{a,min}$  of the DMD process, the adaptive slicing will result in a growing mismatch between the ideal and the actual slicing planes. A certain overhang can be addressed by a five-axis tool path as shown in the following section. Unfeasible overhangs require either a redesign of the part, or a segmentation into sub-volumes with different buildup directions according to slicing approach (b) of Fig. 1.

## 2.2 Five-Axis Tool Path Creation

A machine tool with a minimum of three linear and two rotational axes is required to rotate the processing head in any direction. Here, a CNC machine with three linear axes X, Y, and Z as well as a tilt axis B (around the Y-axis) and a rotation axis C (around the Z-axis) is used. In order to modify the tool axis orientation while maintaining the tool center point (TCP) at the position of the melt pool, the NC controller calculates compensation moves of the linear axes when rotations are performed. In contrast to most robots, a five-axis CNC machine allows an unambiguous transformation between the position and orientation of the TCP and the axes and joints of the machine. A singularity exists at  $B = 0^\circ$ , as it allows an arbitrary C-angle without an effect on the tool axis orientation.

Although the adaptive slicing ensures a normal vector  $\underline{m}_i$  parallel to the average wall direction, parts with a varying cross-section show local overhangs in different directions. For instance, the average wall direction of a cone is constant and parallel to the axis of revolution, but there is still a remaining overhang due to the taper angle as illustrated in Fig. 4 (a). For the fabrication of a thin-walled part by DMD, the direction of the laser beam needs to be parallel to the local wall direction. Otherwise, small deviations of the part height will lead to a mismatch between the position of the laser beam and the actual part surface. Thus, the B and C angles need to be calculated for each tool path segment based on the local STL triangle.

Figure 4 (b) shows the contour path at an arbitrary position  $k$  and layer  $i$ , intersecting a triangle with a normal vector  $\underline{n}_{k,i}$ . The normalized path direction  $\hat{\underline{u}}_{k,i}$  is given as the cross-product of  $\underline{m}_i$  at a position  $k$  and  $\underline{n}_{k,i}$ :

$$\hat{\underline{u}}_{k,i} = \underline{m}_i \times \underline{n}_{k,i} \quad (8)$$

The local wall direction  $\tilde{\underline{m}}_{k,i}$  has an overhang angle  $\beta_p$  relative to the normal vector  $\underline{m}_i$  of the slicing plane and is calculated as:

$$\tilde{\underline{m}}_{k,i} = \underline{n}_{k,i} \times \hat{\underline{u}}_{k,i} \quad (9)$$

With  $\tilde{\underline{m}}_{k,i}$  as the tool axis orientation, the B-tilt angle  $B_{k,i}$  of the machine tool is determined by the z-component of  $\tilde{\underline{m}}_{k,i}$  in the machine coordinate system  $(x, y, z)$ :

$$B_{k,i} = \cos^{-1}(\tilde{m}_{k,i,3}) \quad (10)$$

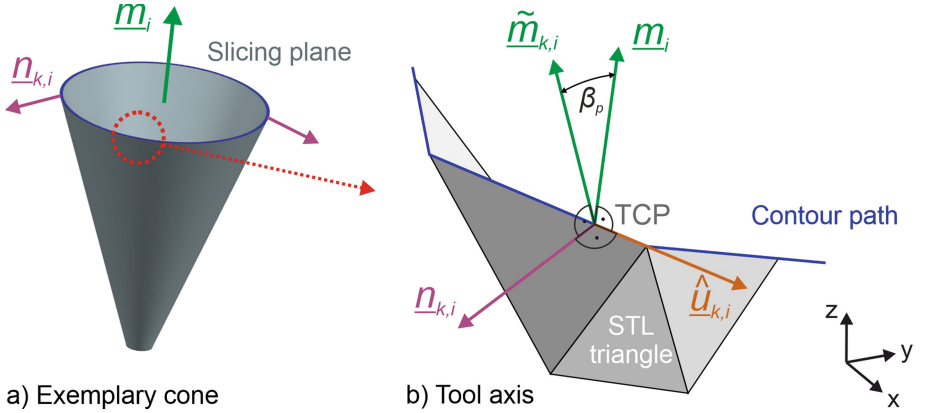


**Fig. 4.** Exemplary cone with overhangs despite adaptive slicing (a), geometric derivation of the tool axis  $\underline{\tilde{m}}_{k,i}$  parallel to the wall (b)

The C-rotation angle  $C_{k,i}$  is given by the x- and y-components of  $\underline{\tilde{m}}_{k,i}$  with the four-quadrant inverse tangent:

$$C_{k,i} = \tan^{-1} \left( \frac{\tilde{m}_{k,i 2}}{\tilde{m}_{k,i 1}} \right) + \frac{\pi}{2} \frac{\tilde{m}_{k,i 2}}{|\tilde{m}_{k,i 2}|} \left( 1 - \frac{\tilde{m}_{k,i 1}}{|\tilde{m}_{k,i 1}|} \right) \quad (11)$$

The local angles  $(B, C)_{k,i}$  are assigned to the current TCP  $(x, y, z)_{k,i}$ , thus the position and orientation of the processing head are defined for each path segment. Knowledge of the actual machine kinematics is not required as far as the NC controller transforms the TCP coordinates into machine coordinates. As a further step before completion of the NC-code, suitable process parameters need to be determined.

### 2.3 Laser Power Adaptation

Especially for the fabrication of thin-walled parts, the processing conditions vary significantly between the bottom and the top of a part: The first layer deposited onto a cold, massive substrate is subjected to high thermal conduction through the workpiece. In contrast, the heat flow and the thermal gradient at the top of a heated, thin-walled part are significantly lower as revealed experimentally by Akbari and Kovacevic [13] for laser/wire AM: They show that the microstructure between the bottom and the top of a thin wall varies highly due to the different cooling rates in different production stages.

In order to ensure comparable melt pool properties for different part geometries and workpiece temperatures, the heat input in terms of the laser power needs to be adapted. This can be done by melt pool monitoring and a closed-loop control, or by a model-based feedforward control as further explained by Eisenbarth et al. [11]: During generation of the NC-code, a digital twin of the part is created that shows the deposited material in each stage of production.



Simultaneously, the local part geometry around the current position of the melt pool is analyzed. Figure 5 illustrates the principle: The algorithm spans a control volume of a fixed size (green) around the melt pool (red). A geometric factor  $\kappa$  indicates the amount of material inside the control volume that is available for thermal conduction. If processing is performed on a massive part,  $\kappa$  equals 1. For a thin wall, the workpiece does not fill the control volume entirely and  $\kappa$  decreases accordingly.

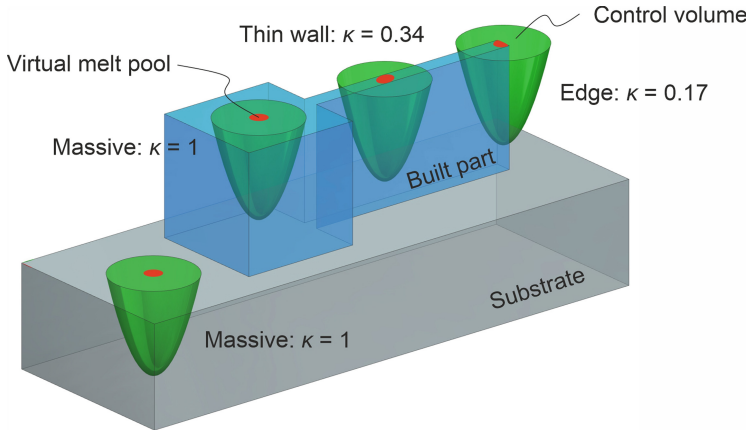


**Fig. 5.** Control volume (green) during fabrication of an exemplary part (blue) on a massive substrate (gray) according to [11]

$\kappa$  is therefore a measure for the massiveness of a part. The geometric factor is then correlated to the required laser power by an experimental calibration with certain test geometries such as a massive block and a thin wall. With suitable laser power values  $P_1$  for  $\kappa = 1$  and  $P_0$  for  $\kappa = 0$  for a specific material and process window, values within these limits are interpolated linearly. Compared to a thermodynamic simulation, a geometry-based algorithm as shown here is fast, can handle complex geometries, and does not rely on advanced material properties. The laser power adaptation is independent of the scan speed adaptation for the adaptive slicing, but all possible combinations of  $P$  and  $v$  are considered for the definition of the process window.

## 2.4 Experimental Setup

For the fabrication of parts, a prototype machine for combined DMD and milling from the Swiss company GF Machining Solutions is used. The CNC machine has a linear axis range of  $X = 600$  mm,  $Y = 450$  mm, and  $Z = 450$  mm. The table rotates  $360^\circ$  around the C-axis and turns from  $-120$  to  $+45^\circ$  around the B-axis. A DMD system type AMBIT from company Hybrid Manufacturing Technologies

with a nominal laser spot size of 3 mm and a maximum laser power of 1000 W at a wavelength of 1070 nm is integrated in the machine. The initial distance from the workpiece to the nozzle is 8 mm. The nickel-base alloy Inconel<sup>®</sup> (IN) 718 from Carpenter Additive is applied exemplarily, as it is easy to weld and suited for high-temperature applications in the energy and aerospace industry. The powder has a particle size distribution from 44 to 105  $\mu\text{m}$ . DMD process parameters are listed in Table 1.

**Table 1.** DMD process parameters for material IN718

Parameter	Value
Min. laser power $P_0$ [W]	480
Max. laser power $P_1$ [W]	1000
Min. scan speed $v_{min}$ [mm/min]	150
Max. scan speed $v_{max}$ [mm/min]	450
Powder flow rate $\dot{m}$ [g/min]	4.6

### 3 Results and Discussion

#### 3.1 Layer Height Calibration

A suitable process window for thin-walled parts from IN718 was determined in pretests with the goal of a pore- and crack-free microstructure. For the calibration of the layer height model according to Eq. (5), straight, thin-walled tubes with a height of 9 mm are fabricated with different scan speeds and a constant laser power  $P_1 = 1000$  W. Figure 6 plots the resulting layer height. The hyperbolic fit proves that  $\delta h$  is inversely proportional to  $v$ . At a scan speed of 150 mm/min, the local layer height is 0.8 mm with a wall thickness  $w_m$  of 3.6 mm. At  $v = 450$  mm/min,  $\delta h$  decreases to 0.3 mm and  $w_m$  decreases slightly to 2.9 mm. Within this window, the specific energy  $e_a$  ranges between 46 and 111 J/mm<sup>2</sup>. The average volumetric energy density  $e_v$  is 147 J/mm<sup>3</sup> with a standard deviation of  $\pm 15$  J/mm<sup>3</sup>. Deviations of  $e_v$  are due to the fact that the powder catchment efficiency  $\eta$  increases with the melt pool size. According to Eq. (6), the volumetric energy density is slightly reduced in areas with a higher wall thickness and powder catchment efficiency. Considering the laser power adaptation,  $e_v$  decreases to 71 J/mm<sup>3</sup> if the minimum laser power  $P_0 = 480$  W is applied.

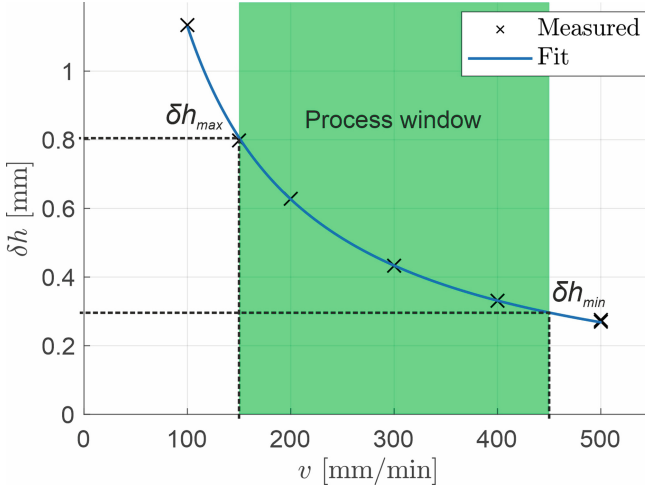


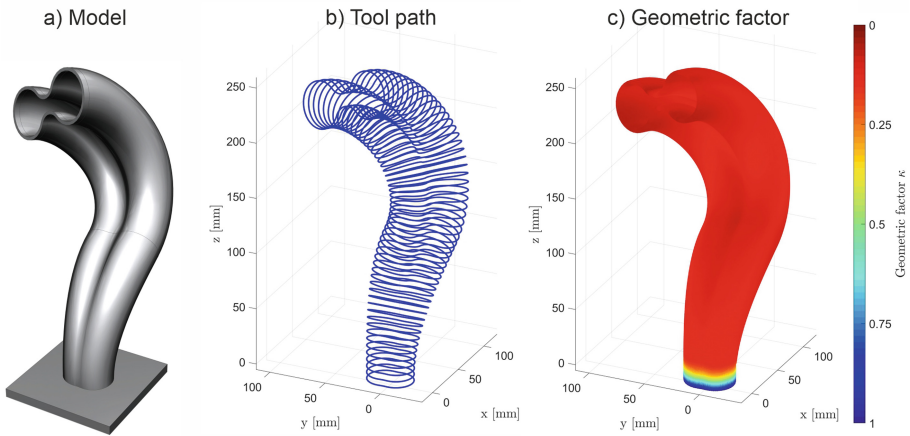
**Fig. 6.** Local layer height  $\delta h$  as a function of the scan speed  $v$

### 3.2 Exhaust Manifold Fabrication

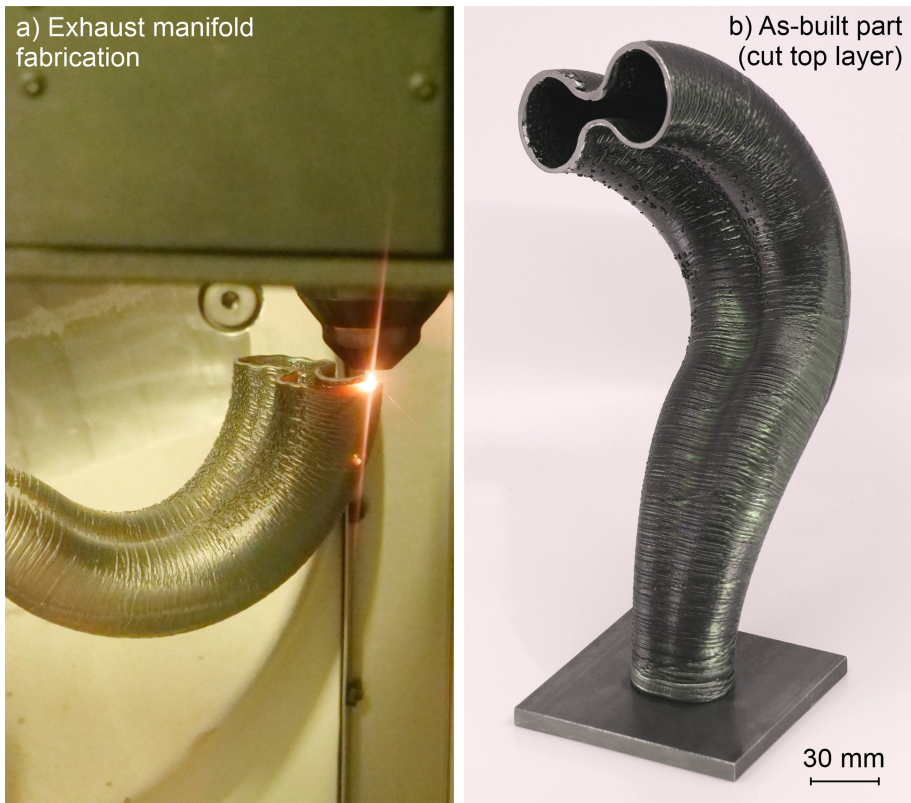
The exhaust manifold is modeled as a sweep of a varying cross-section along a 3D guide curve as shown in Fig. 7 (a). The cross-section starts with an oval shape with a size of 40 times 30 mm, and transitions into an hourglass shape with a size of 96 times 40 mm. In the lower section, the guide curve follows a circular arc in the  $xz$ -plane up to a tilt angle of  $60^\circ$  from the initial  $z$ -direction. In the upper section, the guide curve is reversed and follows a plane that is rotated by  $30^\circ$  relative to the previous  $xz$ -plane. The top layer has a tilt angle of  $-80^\circ$ . The exhaust manifold has a total height of 250 mm and a minimum surface radius  $r_a$  of 18 mm in the tilting direction, which is also the achievable radius  $r_{a,min}$  of the chosen process window.

Figure 7 (b) depicts the tool path, consisting of stacked contours. For clarity reasons, only every 10<sup>th</sup> layer is displayed. The algorithm calculates adapted slicing planes that can follow the curvature of the part, since the model geometry complies with the process limitations. Due to the varying cross-section, local overhangs exist with a maximum angle of  $\beta_p = 15^\circ$ . Picture (c) shows the geometric factor  $\kappa$  in pseudo-colors: In the first layer, processing starts at  $\kappa = 1$  with a laser power of  $P_1 = 1000$  W to ensure a proper bonding to the substrate. After reaching 20 mm wall height, the influence of the substrate on thermal conduction in the thin wall is negligible and  $\kappa$  converges to 0.13 with a corresponding laser power of 550 W, which remains nearly constant until the end of the process.

The fully automated CAM software does not require any engineering work, except of the CAD modeling of the part and the initial parameter development for a specific material. The calculation of the tool path for the exhaust manifold takes 14 min with a desktop PC, using a single core of a 2.5 GHz processor. The DMD process allows a buildup rate of 154 g/h with an average powder catchment



**Fig. 7.** CAM modeling of the exhaust manifold: CAD (a), tool path (b), and geometric factor  $\kappa$  (c)



**Fig. 8.** Exhaust manifold during processing (a), as-built part with cut top layer (b)

efficiency of 57%, resulting in a total weight of the exhaust manifold of 1.2 kg. The fabrication process as depicted in Fig. 8 takes 7 h 50 min. The top layer shows a certain waviness due to process irregularities. The photograph in (b) shows the as-built exhaust manifold, deposited on a 8 mm thick substrate from steel S235JRC. The top layer is cut to show the difference to the dark wall surface, indicating a certain oxidation of IN718. Compared to a planar part, the shield gas stream is less effective on a thin wall. Thus, prevention of any oxidation would require a processing chamber with a controlled shield gas atmosphere.

## 4 Conclusion and Outlook

Deposition welding technologies in combination with a multi-axis CNC machine allow the additive fabrication in arbitrary directions. This publication addresses both the digital and physical challenges of multi-directional AM: An adaptive slicing algorithm is presented that changes the buildup direction gradually. Process parameters in terms of the scan speed and laser power are optimized to account for the characteristics of the DMD process. Thus, the virtual tool path planning is connected to the actual capabilities and limits of the DMD process, shown exemplary for the fabrication of an exhaust manifold. With a CAD model as input, an algorithm calculates the adaptive slicing planes based on the average wall inclination. The remaining overhang is considered by an alignment of the tool axis orientation to the local wall direction. With a five-axis machine tool, the required rotation angles can be calculated unambiguously.

It is shown that the layer height is inversely proportional to the scan speed. Thus, a variable layer height can be realized by a varying scan speed within a certain process window. A model-based feedforward control of the laser power is proposed to adapt the heat input to the changing thermal conduction in thin-walled parts. Finally, the fabrication of a 250 mm high, twisted exhaust manifold from IN718 is shown. The calculation of the required NC-code is performed fully automated based on the CAD model and process parameters for a certain material, reducing the preparation time and effort for a build job significantly.

In the future, the adaptive slicing algorithm should be enhanced for more complex geometries such as splitting and merging parts as well as varying wall thicknesses. The goal is to gain full control of the local layer height for any tool path strategy while ensuring a dense microstructure. A stepwise buildup with intermediate machining and inspection of the internal surfaces would improve the flow properties inside the exhaust manifold.

**Acknowledgements.** The authors would like to acknowledge the contribution of the funding agency Innosuisse (grant number 25498) and of the companies GF Machining Solutions, GF Precicast, and ABB Turbo Systems AG.

## References

1. Greer, C., Nycz, A., Noakes, M., Richardson, B., Post, B., Kurfess, T., Love, L.: Introduction to the design rules for metal big area additive manufacturing. *Additive Manufacturing* **27**, 159–166 (2019). <https://dx.doi.org/10.1016/j.addma.2019.02.016>
2. Petrat, T., Graf, B., Gumenyuk, A., Rethmeier, M.: Laser metal deposition as repair technology for a gas turbine burner made of inconel 718. *Phys. Procedia* **83**, 761–768 (2016). <https://doi.org/10.1016/j.phpro.2016.08.078>
3. Ding, D., Pan, Z., Cuiuri, D., Li, H., Larkin, N., van Duin, S.: Automatic multi-direction slicing algorithms for wire based additive manufacturing. *Robot. Comput. Integr. Manuf.* **37**, 139–150 (2016). <https://doi.org/10.1016/j.rcim.2015.09.002>
4. Murtezaoglu, Y., Plakhotnik, D., Stautner, M., Vaneker, T., van Houten, F.J.A.M.: Geometry-based process planning for multi-axis support-free additive manufacturing. *Procedia CIRP* **78**, 73–78 (2018). <https://doi.org/10.1016/j.procir.2018.08.175>
5. Zhao, G., Ma, G., Feng, J., Xiao, W.: Nonplanar slicing and path generation methods for robotic additive manufacturing. *Int. J. Adv. Manuf. Technol.* **96**(9-12), 3149–3159 (2018). <https://dx.doi.org/10.1007/s00170-018-1772-9>
6. Mao, H., Kwok, T., Chen, Y., Wang, C.: Adaptive slicing based on efficient profile analysis. *Comput. Aided Des.* **107**, 89–101 (2019). <https://doi.org/10.1016/j.cad.2018.09.006>
7. Chalvin, M., Campocasso, S., Baizeau, T., Hugel, V.: Automatic multi-axis path planning for thinwall tubing through robotized wire deposition. *Procedia CIRP* **79**, 89–94 (2019). <https://doi.org/10.1016/j.procir.2019.02.017>
8. Wang, M., Zhang, H., Hu, Q., Liu, D., Lammer, H.: Research and implementation of a non-supporting 3D printing method based on 5-axis dynamic slice algorithm. *Robot. Comput. Integr. Manuf.* **57**, 496–505 (2019). <https://doi.org/10.1016/j.rcim.2019.01.007>
9. Ruan, J., Eiamsa-ard, K., Liou, F.W.: Automatic process planning and toolpath generation of a multiaxis hybrid manufacturing system. *J. Manuf. Processes* **7**(1), 57–68 (2005). [https://doi.org/10.1016/S1526-6125\(05\)70082-7](https://doi.org/10.1016/S1526-6125(05)70082-7)
10. Wang, X., Liu, Z., Guo, Z., Hu, Y.: A fundamental investigation on three-dimensional laser material deposition of AISI316L stainless steel. *Opt. Laser Technol.* **126**, 106107 (2020). <https://dx.doi.org/10.1016/j.optlastec.2020.106107>
11. Eisenbarth, D., Soffel, F., Wegener, K.: Geometry-based process adaption to fabricate parts with varying wall thickness by direct metal deposition. In: *Progress in Digital and Physical Manufacturing, Progress in Digital and Physical Manufacturing*, pp. 125–130. Springer, Leiria (2020). [https://doi.org/10.1007/978-3-030-29041-2\\_16](https://doi.org/10.1007/978-3-030-29041-2_16)
12. Ruan, J., Sparks, T.E., Panackal, A., Liou, F.W., Eiamsa-ard, K., Slattery, K., Chou, H.N., Kinsella, M.: Automated slicing for a multiaxis metal deposition system. *J. Manuf. Sci. Eng.* **129**(2), 303–310 (2006). <http://dx.doi.org/10.1115/1.2673492>
13. Akbari, M., Kovacevic, R.: An investigation on mechanical and microstructural properties of 316lsi parts fabricated by a robotized laser/wire direct metal deposition system. *Addit. Manuf.* **23**, 487–497 (2018). <https://doi.org/10.1016/j.addma.2018.08.031>